Non-Precious-Metal Catalyst

DOI: 10.1002/anie.201204958

Iron Encapsulated within Pod-like Carbon Nanotubes for Oxygen Reduction Reaction**

Dehui Deng, Liang Yu, Xiaoqi Chen, Guoxiong Wang, Li Jin, Xiulian Pan, Jiao Deng, Gongquan Sun, and Xinhe Bao**

Efforts to explore non-precious-metal cathode catalysts to replace the precious Pt in polymer electrolyte membrane fuel cells (PEMFC) have been going on for several decades to bring this efficient technology into real applications. Progress has been made through the use of macrocyclic molecules particularly those containing Fe-N_4 and Co-N_4 moieties, or high-temperature synthetic materials containing separately or collectively transition-metal/nitrogen/carbon elements.[1–7] However, the non-precious-metal based catalysts frequently suffer from poor stability in acids owing to leaching.[3,8] Recently, Wu et al. reported an encouraging catalyst synthesized from high-surface-area carbon, polyaniline, iron and cobalt at a high temperature, which exhibited a high activity and stability as an oxygen reduction reaction (ORR) catalyst in PEMFC. The metal-containing particles were to a large extent encapsulated in onion-like carbon nanoshells or attached to carbon nanosheets.[9] However, the nature of the active ORR catalytic sites was not clear. Our previous study demonstrated that the coordinatively unsaturated ferrous sites, when confined on the interface of Pt, are highly active and stable in activating oxygen.[10] Herein we intend to design active and stable non-precious metal ORR catalysts with features of coordinatively unsaturated metal sites or low valence state metals physically isolated from the acid environment to avoid leaching, which however should not impede the catalytic properties of metals, and on this basis, to understand the behavior of active sites.

[*] Dr. D. H. Deng, Dr. L. Yu, X. Q. Chen, Dr. G. X. Wang, L. Jin, Prof. X. L. Pan, J. Deng, Prof. X. H. Bao
State Key Laboratory of Catalysis, Dalian Institute of Chemical Physics, Chinese Academy of Sciences
Zhongshan Road 457, Dalian 116023 (China)
E-mail: panxl@dicp.ac.cn
xhbao@dicp.ac.cn
Homepage: http://fruit.dicp.ac.cn/
Prof. G. Q. Sun
Laboratory of Fuel Cell
Dalian Institute of Chemical Physics, Chinese Academy of Sciences
Zhongshan Road 457, Dalian 116023 (China)

[**] We gratefully acknowledge the financial support from the Ministry of Science and Technology of China (No. 2011CBA00503 and 2012CB215500) and the National Science Foundation of China (No. 11079005 and 21033009), and the assistance from Shanghai Synchrontron Radiation Facilities during in situ XANES studies. We thank Hongmei Yu and Ming Hou for help in PEMFC sulfur resistance tests, and Peijun Hu, Meiyin Chou, and Fan Yang for fruitful discussions.

Supporting information for this article is available on the WWW under http://dx.doi.org/10.1002/anie.201204958.

We encapsulated Fe nanoparticles into the compartments of pea-pod like carbon nanotubes (CNTs) through one-step synthesis at 350 °C in N_2 using ferrocene and sodium azide as the precursors (see Experimental Section in Supporting Information). This method allows scalable synthesis with good reproducibility. Fe particles outside of the carbon shells were removed by thorough washing in acid solution, and the resulting sample is denoted as Pod-Fe. Scanning electron microscope (SEM) images (Figure S1 in the Supporting Information) and transmission electron microscopy (TEM) images (Figure 1 a,b and Figure S2) show that the Pod-Fe sample exhibits a well-defined pea-pod-like structure and the graphitic wall ranges between about 1 to 8 layers with a layer distance of 3.40 ± 0.05 Å. The Fe nanoparticles are completely isolated within the compartments of CNTs and each compartment usually contains 1–2 Fe particles. No particles are observed on the outer shells of CNTs when scanning randomly across the sample under the electron microscope. X-ray photoelectron spectroscopy (XPS; Figure S3 and Table S2) analysis indicates the presence of iron, carbon, and oxygen in Pod-Fe but with a negligible content of nitrogen. These nanoparticles in CNTs exhibit a *d* spacing of 2.04 ± 0.05 Å, corresponding to the [110] plane of metallic Fe, as shown by the high resolution TEM (HRTEM) image (Figure 1 b and its inset). No other phases are observed in the X-ray diffraction (XRD) pattern of Pod-Fe (Figure 1 c). The metallic state of the confined iron is further corroborated by X-ray absorption near-edge spectra (XANES) of Fe K-edge (Figure 1 d), which is sensitive to the chemical state of atoms. In comparison, the spectrum for the sample before acid washing, denoted as FeO_x/Pod-Fe, indicates the presence of oxide, as also detected by XRD (Figure 1 c) and XPS (Figure S3). These results confirm the complete encapsulation of metallic Fe inside CNTs, which prevents Fe from being oxidized even after prolonged exposure to air.

The rotating-disk electrode (RDE) test in acidic electrolyte indicates that Pod-Fe is significantly more active in ORR than CNTs and commercial Vulcan XC-72 (Figure S4). Pod-Fe was then assembled into a cathode and tested in a single H_2–O_2 fuel cell with a Fe loading of 0.38 mg cm^{-2} while the anode consisted of a commercial 20 % Pt/C catalyst from Johnson Matthey (JM) with a Pt loading of 0.20 mg cm^{-2}. Figure 2 a shows that at 80 °C and 3.0 bar at the cathode, the cell yields a voltage of 0.34 V at a current of 0.10 A cm^{-2}, which is 40 % of that given by 20 % Pt/C cathode at the same current density. During 210 h on stream (Figure 2 b), the voltage declines only by about 8 % from the initial 0.25 V (averaged for the first 10 h). When the discharge is stopped and the cell is restarted, the voltage can be restored to the

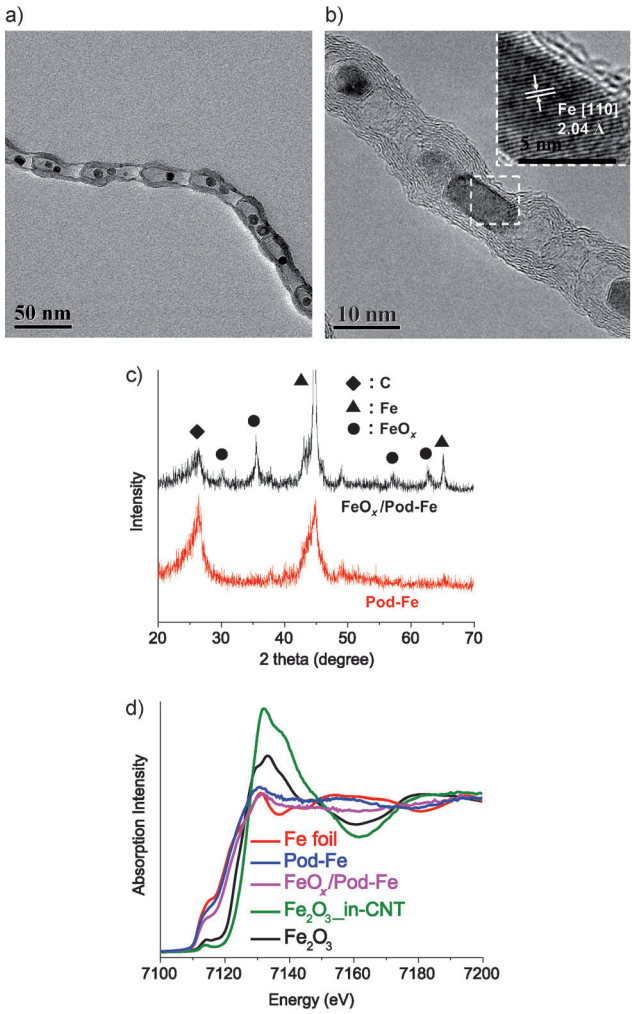

Figure 1. a) TEM image of Pod-Fe; b) HRTEM image of Pod-Fe with the inset showing the [110] crystal plane of the Fe particle; c) XRD patterns of Pod-Fe in comparison to FeO_x/Pod-Fe; d) Fe K-edge XANES of Pod-Fe in comparison to FeO_x/Pod-Fe, Fe foil, Fe_2O_3, and Fe_2O_3-in-CNT in which Fe_2O_3 nanoparticles are distributed inside CNTs with open channels, prepared according to our previous report.[11]

initial value, indicating that Pod-Fe maintains its ORR activity fairly well under the PEMFC operation conditions.

Previous reports indicate the presence of nitrogen in the iron/carbon composites can enhance the ORR activity.[6,7,9,12] Inspired by this, we used $(NH_4)_4Fe(CN)_6{\cdot}xH_2O$ as the precursor and synthesized Pod(N)-Fe (see Experimental Section in Supporting Information), which contains 2.4 wt.% of N in the structure (Figure S10 and Table S2). Similarly, metallic Fe particles are encapsulated within the graphitic carbon compartments (Figure S7, S9). Indeed, Pod(N)-Fe exhibits a much higher ORR activity (Figure 2a, S4) compared to Pod-Fe and also a long-term stability when tested under both steady current (Figure 2b) and steady voltage modes (Figure S5) in PEMFC. Figure 2a and Figure S4 show that the activity can be further enhanced by encapsulating CoFe alloy within N-doped Pod-like CNTs (Pod(N)-FeCo, Figure S8–10). The voltage has increased to 60% of that given by 20% Pt/C cathode at the current of 0.10 A cm^{-2} in PEMFC. Both Pod(N)-Fe and Pod(N)-FeCo catalysts deliver a fairly stable cell performance for more than 220 h (Figure 2b).

Nanosized iron particles are susceptible to oxidation. However, in situ XANES in Figure 2c reveals an intact metallic iron in Pod-Fe after running for 7 h in PEMFC. TEM examination does not show any visible change in the morphology of the used catalyst. Note that Pt is very sensitive even to trace SO_2, which can significantly reduce the performance of a PEMFC and thus has recently stimulated wide interest in developing sulfur-resistant catalysts.[13–15] Figure 2d shows that the cell operates rather stably with Pod-Fe cathode, Pod(N)-Fe, and Pod(N)-FeCo even in the presence of 10 ppm SO_2 in air. In contrast, it deteriorates quickly and the voltage drops about 40% within 1 h with the 20% Pt/C cathode. In situ XANES (Figure S11b) does not detect the iron sulfide species on the cathode and iron in Pod-Fe remains metallic even after 8 h exposure to SO_2, while bisulfate or sulfate species were observed recently on nanoscale Pt particles.[16] These results indicate that iron is well shielded by CNT walls against O_2, SO_2, and the acid environment, leading to a stable performance in PEMFC.

CN^- ions can coordinate strongly to Fe and poison the iron-based sites for ORR.[17,18] However, we found the presence of CN^- ions does not reduce the ORR activity of Pod-Fe, which further confirms that the outer surface of Pod-Fe is free of Fe species (Figure S12). Surprisingly, such physically isolated Fe nanoparticles within carbon compartments are active for ORR even though oxygen is not in direct contact with Fe. Therefore, the encapsulated Fe nanoparticles must have interacted with the CNT shell and affected the properties of the outer wall where O_2 is activated and reduced, as shown in in Figure 3c. To understand the origin of the ORR activity of Pod-Fe, we carried out density function theory (DFT) calculations, and further experiments using UV laser enhanced photoemission electron microscopy (PEEM).

Models containing a Fe_4 nanoparticle inside a (6,6) single-walled carbon nanotube (Fe_4@SWNT, Figure 3a) and a double-walled carbon nanotube (DWNT) (6,6)@(11,11) (Figure S16a) are used in DFT calculations. Although the sizes of the Fe nanoparticle and the nanotube considered in the calculations are much smaller than the Fe nanoparticles and nanotubes observed experimentally, the essential effect on the electronic structure, as shown below, can already be captured by this simple geometry. Figure 3a shows the projected density of states (DOS) for the p orbital of the C atoms bonded to Fe_4 (marked in inset I) compared with the DOS of the pristine SWNT. Based on the results in Figure 3a, two effects can be identified arising from the Fe–C interaction in Fe_4@SWNT. First, states associated with the C atoms close to the Fe cluster are significantly modified in the energy range from −7.5 to −3.5 eV, exhibiting extra features in the characteristic low-DOS region near the Fermi level for a metallic SWNT. Second, a charge transfer from the Fe cluster to the SWNT takes place and Bader charge analysis shows that 1.45 electrons are transferred from Fe_4 to carbon, raising the Fermi level by about 0.5 eV. This effect is further illustrated by the difference charge–density distribution as shown in the inset II of Figure 3a, in which an increase of the

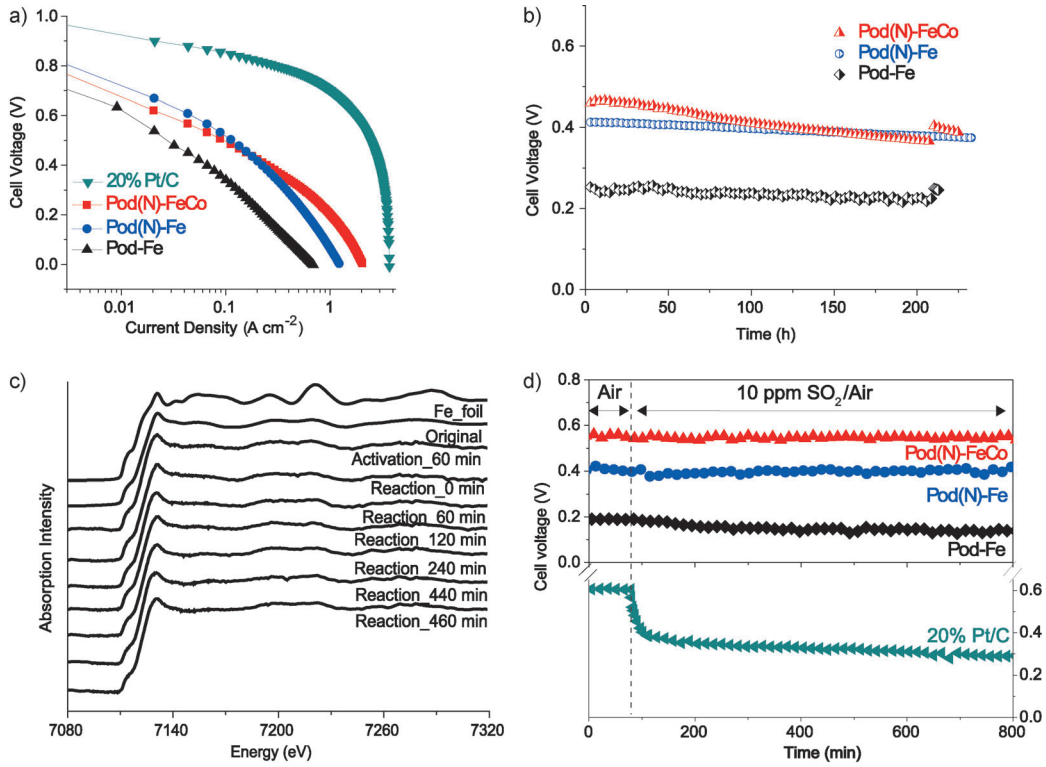

Figure 2. a) A single H_2–O_2 fuel cell performance test with Pod-Fe, Pod(N)-Fe, Pod(N)-FeCo, and commercial 20% Pt/C (JM) cathodes. b) H_2–O_2 fuel cell durability test with the Pod-Fe, Pod(N)-Fe, Pod(N)-FeCo cathodes at a steady current of 0.1, 0.5, and 0.5 A, respectively (Pod-Fe at 70°C and 2.0 bar). c) In situ Fe K-edge XANES of Pod-Fe cathode under PEMFC operation conditions. d) Durability test in presence of 10 ppm SO_2 in air, with the Pod-Fe, Pod(N)-Fe, Pod(N)-FeCo cathodes at a steady current 0.05, 0.1, and 0.1 A, respectively, compared to 20% Pt/C (JM) at 3.0 A (70°C and 2.0 bar) with the Pt loading of 0.2 mg cm^{-2}. Single-cell tests of Pod-Fe, Pod(N)-Fe, Pod(N)-FeCo, and 20% Pt/C are carried out at 80°C and 3.0 bar at both anode and cathodes, unless stated otherwise.

p_z charge density can be clearly seen at the C atoms surrounding the Fe cluster. In addition, the charge transfer will also be accompanied by the formation of a local dipole near the surface. The overall modification is expected to decrease the local work function and increase the chemical reactivity of the functionalized region of the SWNT exterior. Figure 3a and the inserted image III indicate that doping nitrogen atoms into the carbon lattice in the region where iron is sitting below can further increase the DOS near Fermi level and reduce the work function of the doped area.

Further results show that O_2 can be readily adsorbed on the carbon layer of Fe_4@SWNT and the adsorption free energy is 0.03 eV and remarkably more negative than the 1.43 eV on the pristine SWNT. This change is attributed to the promoted charge transfer from carbon to oxygen which favors both the electrostatic and covalent bonding between them on the carbon layer encapsulating Fe_4 (see DFT Calculation Section in Supporting Information). Upon N doping on SWNT (Fe_4@N-SWNT), the adsorption free energy further decreases to −0.44 eV, denoting that incorporation of N can notably facilitate the O_2 adsorption. On these sites O_2 can be converted into H_2O following an associative mechanism (Figure 3b), which is similar to our previous observation on (N-doped) graphene.[20,21] The process goes via a four electron transfer pathway with the highest barrier of 0.68 eV under PEMFC operation conditions (see DFT Calculation Section in Supporting Information for more details), which is in accordance with our rotating ring disk electrode (RRDE) results (Figure S6 and Table S1). Furthermore, the electron transfer from the encapsulated Fe_4 cluster can extend from the inner to the outer tube in DWNT (6,6)@(11,11), resulting in an increased charge density on the outer (11,11) tube, as demonstrated in Figure S16a. Although it is not clear yet from the current theoretical calculations whether the modification of electronic structures can be extended through more than three carbon layers due to the limitation of the computing capability, our PEEM enhanced by UV laser as exciting light shows the possibility.

The interaction of Fe nanoparticles with the graphitic walls of CNTs may change their local work function, as was found for CNTs decorated with Ru nanoparticles, as a result of electron transfer from Ru to CNTs.[22,23] Thus, we expect that the PEEM, a tool highly sensitive to the change of local work function, could provide a direct confirmation of the work function change discussed above. The PEEM image in Figure 4a shows a significantly bright contrast at one spot along with the tube. The low-energy electron microscopy (LEEM) image, which reflects the surface morphology, of the same region of this specimen confirms an intact tube without exotic particles (the inset of Figure 4a). Therefore, this spot in the PEEM image could correspond to Fe particles encapsulated in CNTs, which suggests a decreased work function at this region, as the result of the interaction between the encapsulated Fe particles with the graphitic carbon of CNTs.

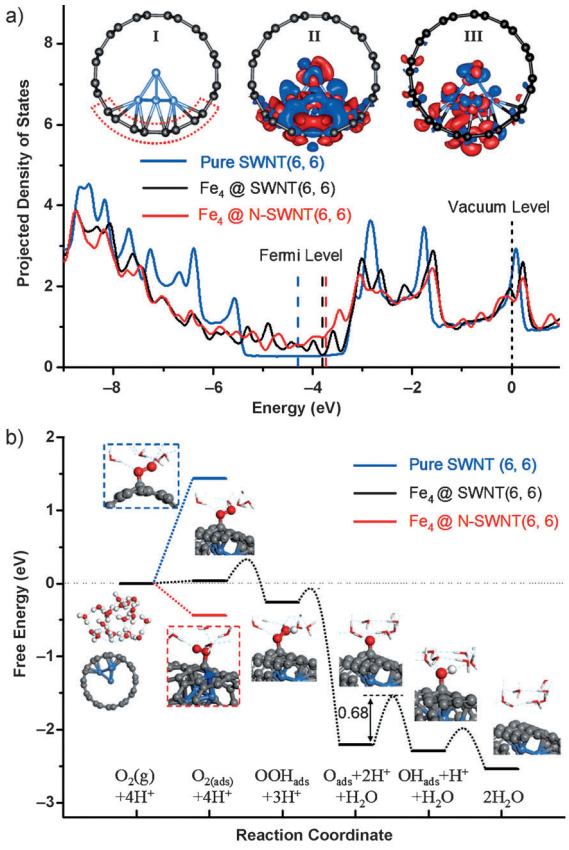

Figure 3. Results of DFT calculations: a) Projected DOS of the p orbitals of C atoms bonded to Fe_4 in Fe_4@SWNT and Fe_4@N-SWNT compared with that in pure SWNT. The vacuum level is aligned at 0 eV. Inserted plot I and plot II show the optimized structure of Fe_4@SWNT and its difference charge density, and Figure S18 and plot III correspond to that of Fe_4@N-SWNT.[19] The red and blue regions in plot II and III indicate a charge increase and decrease, respectively. b) Free-energy diagram of ORR on Fe_4@SWNT in water (black line) under experimental conditions (onset potential = 0.6 V vs. normal hydrogen electrode (NHE), pH 0). c) A schematic representation of the ORR process at the surface of Fe_4@SWNT. The gray C, red O, white H and yellow Fe atoms.

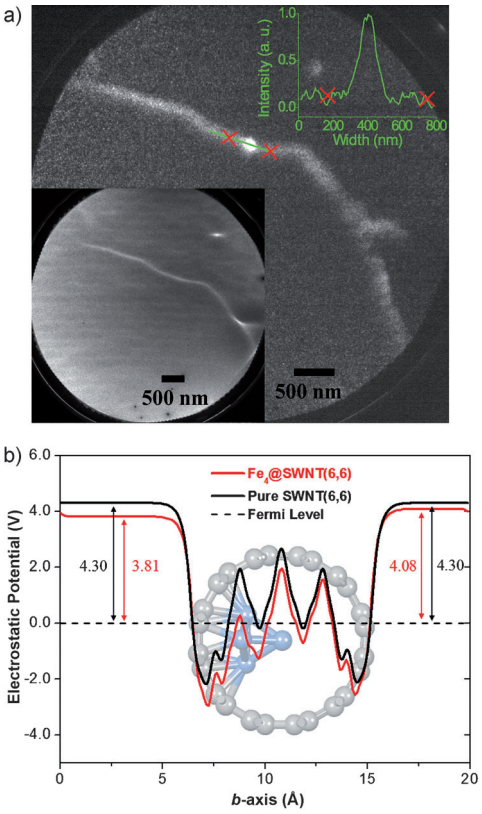

Figure 4. a) PEEM image of Pod-Fe with a start voltage of 1.7 V for its laser. The top inset showing the brightness profile along the green line. The bottom inset showing the corresponding LEEM image of the same region. b) The electrostatic potential profiles averaged on the plane perpendicular to *b*-axis as a function of the *b*-axis of the supercell of Fe_4@SWNT and pure SWNT, respectively. The structure of Fe_4@SWNT is shown in the back ground.

Theoretical calculations (Figure 4b) shows that upon encapsulating Fe_4 in SWNT (6,6), the work function decreases by about 0.5 eV from 4.3 eV at the carbon surface bonded with Fe_4. Although the variation of work function decreases with the increasing number of carbon layers, the decrease for Fe_4@DWNT is still about 0.1 eV (Figure S16b). The reduced local work function at the carbon surface with iron sitting below is expected to enhance its chemical activity. This expectation is confirmed by oxidizing Pod-Fe in air at high temperature (400 °C). TEM images in Figure S14 show that carbon layer in contact with the encapsulated Fe particle is oxidized prior to the region without Fe particles, suggesting that the region in contact with the nanoparticles is more active than the region without nanoparticles, providing further evidence for the analysis in DFT calculations and PEEM studies.

In summary, metallic Fe nanoparticles have been encapsulated within the compartments of pea-pod like CNTs through one step synthesis. The unique morphology of such a composite provides a well-defined model for understanding the nature of Fe-based cathode catalysts in PEMFC. In this system, direct contact of metal particles with harsh environments including acid medium, oxygen, and sulfur contaminations is avoided. However, this protection does not impede the activation of O_2 and the catalyst has a rather high activity and long-term stability in PEMFC even in the presence of SO_2 poison. DFT calculations indicate that the catalytic activity could arise from the electron transfer from Fe particles to the CNTs leading to a decreased local work function on the carbon surface. Interestingly, doping N into the carbon lattice

further increases the DOS near Fermi level and reduces the local work function, and experiments show a significantly enhanced ORR activity. These findings provide a new concept in designing efficient and durable electrocatalysts, as well as heterogeneous catalysts under harsh reaction conditions.

Received: June 25, 2012
Revised: September 11, 2012
Published online: December 6, 2012

Keywords: carbon nanotubes · heterogeneous catalysis · iron · nanoparticles · oxygen reduction reaction

[1] R. Bashyam, P. Zelenay, *Nature* **2006**, *443*, 63 – 66.
[2] R. Borup, J. Meyers, B. Pivovar, Y. S. Kim, R. Mukundan, N. Garland, D. Myers, M. Wilson, F. Garzon, D. Wood, et al., *Chem. Rev.* **2007**, *107*, 3904 – 3951.
[3] M. Lefevre, E. Proietti, F. Jaouen, J. P. Dodelet, *Science* **2009**, *324*, 71 – 74.
[4] F. Jaouen, E. Proietti, M. Lefevre, R. Chenitz, J.-P. Dodelet, G. Wu, H. T. Chung, C. M. Johnston, P. Zelenay, *Energy Environ. Sci.* **2011**, *4*, 114 – 130.
[5] Z. Chen, D. Higgins, A. Yu, L. Zhang, J. Zhang, *Energy Environ. Sci.* **2011**, *4*, 3167 – 3192.
[6] E. Proietti, F. Jaouen, M. Lefevre, N. Larouche, J. Tian, J. Herranz, J.-P. Dodelet, *Nat. Commun.* **2011**, *2*, 416.
[7] S. Gupta, D. Tryk, I. Bae, W. Aldred, E. Yeager, *J. Appl. Electrochem.* **1989**, *19*, 19 – 27.
[8] G. E. Haslam, X.-Y. Chin, G. T. Burstein, *Phys. Chem. Chem. Phys.* **2011**, *13*, 12968 – 12974.
[9] G. Wu, K. L. More, C. M. Johnston, P. Zelenay, *Science* **2011**, *332*, 443 – 447.
[10] Q. Fu, W. X. Li, Y. X. Yao, H. Y. Liu, H. Y. Su, D. Ma, X. K. Gu, L. M. Chen, Z. Wang, H. Zhang, B. Wang, X. H. Bao, *Science* **2010**, *328*, 1141 – 1144.
[11] W. Chen, X. L. Pan, M. G. Willinger, D. S. Su, X. H. Bao, *J. Am. Chem. Soc.* **2006**, *128*, 3136 – 3137.
[12] G. Liu, X. Li, P. Ganesan, B. N. Popov, *Appl. Catal. B* **2009**, *93*, 156 – 165.
[13] J. Fu, M. Hou, C. Du, Z. Shao, B. Yi, *J. Power Sources* **2009**, *187*, 32 – 38.
[14] Y. Zhai, G. Bender, S. Dorn, R. Rocheleau, *J. Electrochem. Soc.* **2010**, *157*, B20 – B26.
[15] J. Zhai, M. Hou, H. Zhang, Z. Zhou, J. Fu, Z. Shao, B. Yi, *J. Power Sources* **2011**, *196*, 3172 – 3177.
[16] D. E. Ramaker, D. Gatewood, A. Korovina, Y. Garsany, K. E. Swider-Lyons, *J. Phys. Chem. C* **2010**, *114*, 11886 – 11897.
[17] S. Gupta, C. Fierro, E. Yeager, *J. Electroanal. Chem.* **1991**, *306*, 239 – 250.
[18] Y. Li, W. Zhou, H. Wang, L. Xie, Y. Liang, F. Wei, J.-C. Idrobo, S. J. Pennycook, H. Dai, *Nat. Nanotechnol.* **2012**, *7*, 394 – 400.
[19] The difference charge density in inserted plot II in Figure 3a is calculated by $\rho_{Fe4@SWNT}-\rho_{Fe4}-\rho_{SWNT}$, where $\rho_{Fe4@SWNT}$, ρ_{Fe4}, and ρ_{SWNT} are the total charge density of Fe_4@SWNT, Fe_4, and SWNT, respectively; that in plot III is calculated by $[\rho_{Fe4@N\text{-}SWNT}-\rho_{Fe4@SWNT}]-[\rho_{N\text{-}SWNT}-\rho_{SWNT}]$, where $\rho_{Fe4@N\text{-}SWNT}$, $\rho_{Fe4@SWNT}$, $\rho_{N\text{-}SWNT}$, and ρ_{SWNT} are the total charge density of Fe_4@N-SWNT, Fe_4@SWNT, N-SWNT, and SWNT, respectively.
[20] D. Deng, L. Yu, X. Pan, S. Wang, X. Chen, P. Hu, L. Sun, X. Bao, *Chem. Commun.* **2011**, *47*, 10016 – 10018.
[21] L. Yu, X. Pan, X. Cao, P. Hu, X. Bao, *J. Catal.* **2011**, *282*, 183 – 190.
[22] C. Liu, K. S. Kim, J. Baek, Y. Cho, S. Han, S.-W. Kim, N.-K. Min, Y. Choi, J.-U. Kim, C. J. Lee, *Carbon* **2009**, *47*, 1158 – 1164.
[23] S. Guo, X. Pan, H. Gao, Z. Yang, J. Zhao, X. Bao, *Chem. Eur. J.* **2010**, *16*, 5379 – 5384.

